Self-Sustained Divertor Oscillation Driven by Magnetic Island Dynamics in Torus Plasma

T. Kobayashi,[1,2] M. Kobayashi,[1,2] Y. Narushima,[1,2] Y. Suzuki,[3,1,2] K. Y. Watanabe,[1,4] K. Mukai,[1,2] and Y. Hayashi[1]

[1]National Institute for Fusion Science, National Institutes of Natural Sciences, Toki 509-5292, Japan
[2]The Graduate University for Advanced Studies, SOKENDAI, Toki 509-5292, Japan
[3]Graduate School of Advanced Science and Engineering, Hiroshima University, Higashi-Hiroshima 739-8527, Japan
[4]Nagoya University, Graduate School of Engineering, Nagoya 464-8603, Japan

(Received 21 September 2021; revised 10 December 2021; accepted 12 January 2022; published 23 February 2022)

A new type of self-sustained divertor oscillation is discovered in the Large Helical Device stellarator, where the peripheral plasma is detached from material diverters by means of externally applied perturbation fields. The divertor oscillation is found to be a self-regulation of an isolated magnetic field structure (the magnetic island) width induced by a drastic change in a poloidal inhomogeneity of the plasma radiation across the detachment-attachment transitions. A predator-prey model between the magnetic island width and a self-generated local plasma current (the bootstrap current) is introduced to describe the divertor oscillation, which successfully reproduces the experimental observations.

DOI: 10.1103/PhysRevLett.128.085001

Isolation of magnetically confined high-temperature plasmas from material walls by manipulating magnetic topology, namely, the divertor plasma operation, is a promising scenario for achieving the fusion relevant reactor condition. In such plasmas, including tokamaks and stellarators, reconciling a high core plasma performance and tolerable heat load onto a divertor target is a great challenge for steady state reactor development. A divertor detachment operation, in which a radiative boundary plasma in front of the divertor target mitigates the direct heat flux, is a viable solution for this issue, and establishment of a stable detachment scenario is highly desirable [1–4]. However, since the divertor detachment is a nonlinear phenomenon, emerging bifurcation [5] or self-sustained oscillation [6,7] is often observed. On the one hand, those are potential obstacles for acquiring the steady state detachment operation. On the other hand, they provide an opportunity to untangle the background nonlinear physics of the detachment [8,9]. Specifically, a multivalued relation between temperature and particle number in the divertor region is suggested [8] to be essential for understanding the recycling driven self-sustained divertor oscillation in tokamaks [6,7]. Externally driven three-dimensional magnetic field perturbation is an attractive control knob for the detachment operation utilized both in tokamaks [10–12] and stellarators [3]. How the plasma responds to the applied magnetic field perturbation, often forming a magnetic island (an closed magnetic flux topology embed into the main magnetic surfaces) [13,14], altering the radiation structure, is an issue to be resolved for obtaining a physics-based detachment control manner.

In this Letter, a new type of self-sustained divertor oscillation discovered in the Large Helical Device (LHD) stellarator under a resonant magnetic perturbation (RMP) application is reported. Since a bifurcative oscillation of 40 Hz is observed among the divertor flux, the radiation loss, and the magnetic island width, the oscillation is regarded to be a sequential repetition of the detachment-attachment transition and back transition. The oscillation likely originates in the upstream plasma, unlike the recycling driven divertor oscillation [6–8]. Nonlinear mutual interaction between the magnetic island and the bootstrap current (self-generated current due to collisions between trapped and passing electrons) is modeled as a predator-prey system. Linear analysis and direct simulation support the validity of the model. Predator-prey models are utilized in different science fields, not only in ecology [15], but also in astronomy [16], dusty plasma physics [17], as well as plasma turbulence physics [18], for describing the competitive relationship among different species. It is demonstrated that the divertor oscillation observed here is an autonomous system in a nonequilibrium open system having a mathematical structure analogous to the above examples.

LHD has a helical confinement magnetic field with toroidal and poloidal field periods of 10 and 2, respectively, which is fully produced by superconducting helical coils. An intrinsic helical double-null divertor configuration is utilized, which is connected to graphite divertor targets.

Published by the American Physical Society under the terms of the Creative Commons Attribution 4.0 International license. Further distribution of this work must maintain attribution to the author(s) and the published article's title, journal citation, and DOI.

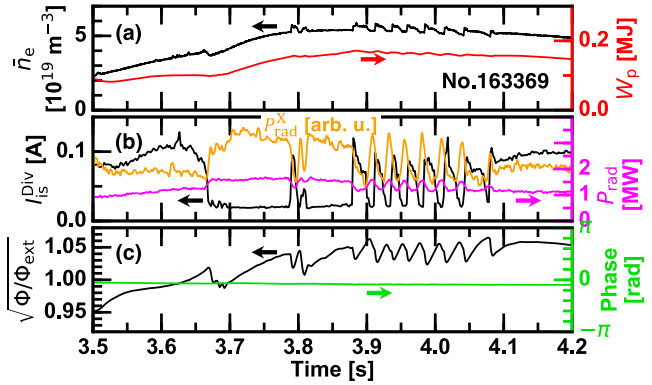


FIG. 1. Time evolutions of (a) line averaged density and plasma stored energy, (b) divertor ion saturation current, total radiation intensity, and X-point radiation intensity, and (c) normalized amplitude and phase of $m/n = 1/1$ radial magnetic field structure.

Divertor detachment assisted by a RMP field is achieved with an outward shifted magnetic axis of $R_{ax} = 3.9$ m and a toroidal field strength of $B_\phi = 2.54$ T (directed counter clockwise viewed from above). In this magnetic configuration, a layer of intrinsic small magnetic islands surrounding closed magnetic surfaces, the so-called stochastic region, emerges in the plasma periphery. Ten pairs of RMP coils are installed at the top and bottom of the device, and produce an $n/m = 1/1$ resonant field at the plasma periphery, where m and n denote the poloidal and toroidal mode numbers [3]. The RMP field often leads to the density pump-out. The transition to divertor detachment in LHD generally occurs when the RMP field fully penetrates into the flux surface with a resonant rotational transform of $\iota/2\pi \equiv 1/q = 1$, where q is the safety factor. Enhanced divertor radiation is initiated once the edge electron temperature drastically drops at the X-point region of the magnetic island [3,19].

Figure 1 shows the time evolution of plasma parameters in the target discharge (No. 163369). The plasma is sustained by three tangentially injected neutral beams of the total input power of 6 MW. From the beginning of the discharge the plasma density is ramped up, and the detachment transition eventually occurs at $t \sim 3.65$ s, where reduction of the divertor ion saturation current and enhancement of the X-point radiation loss are evident [Fig. 1(b)]. Here, a bolometer fan array signal whose line of sight passes through the X-point region is displayed representing the X-point radiation loss. The magnetic island width W normalized by the vacuum RMP island width δ is approximated as $W/\delta = \sqrt{\Phi/\Phi_{ext}}$ according to the magnetohydrodynamic (MHD) equilibrium equation [20], where Φ is the amplitude of the perturbation radial flux and Φ_{ext} is the vacuum RMP flux. Here, the radial magnetic flux is measured with a saddle loop coil array, which has 12 poloidal channels [14]. The detachment transition occurs several tens of milliseconds after the magnetic island width

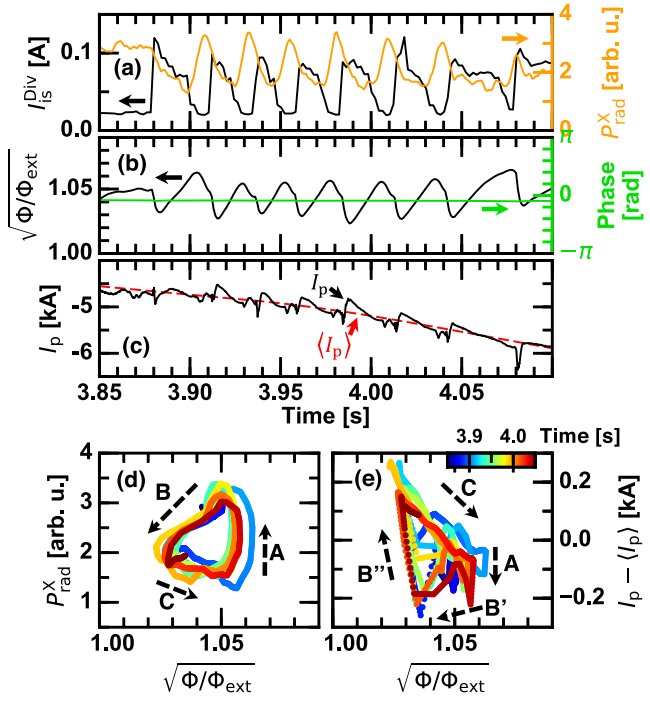


FIG. 2. Time evolutions of (a) divertor ion saturation current and X-point radiation intensity (P^X_{rad}), (b) normalized amplitude ($\sqrt{\Phi/\Phi_{ext}}$) and phase of the $m/n = 1/1$ radial magnetic field structure, (c) plasma current (I_p) and its slowly varying component obtained with 10 Hz low-pass filtering ($\langle I_p \rangle$), and Lissajous diagrams of (d) P^X_{rad} versus $\sqrt{\Phi/\Phi_{ext}}$ and of (e) $I_p - \langle I_p \rangle$ versus $\sqrt{\Phi/\Phi_{ext}}$.

exceeds the vacuum magnetic island width. Immediately after the detachment transition, the magnetic island slightly shrinks, which is a counteraction of the detachment transition. During the discharge, the poloidal location of the magnetic island remains unchanged as shown in Fig. 1(c). The larger the magnetic island becomes, the more the detachment transition is facilitated [21]. As the magnetic island expands, radial transport across the O-point is reduced. In turn, parallel transport along the magnetic island separatrix is relatively enhanced. At the detachment transition, the electron density increases and the electron temperature drops particularly at the X-point region of the magnetic island due to an impurity accumulation at the X-point on the magnetic island separatrix [22]. As a result, impurity radiation at the X-point region is enhanced and the divertor heat flux is mitigated [3,19]. A sequential repetition of the detachment transition and back transition begins at $t \sim 3.875$ s with a repetition frequency of ~40 Hz. This oscillation is also visible in plasma global parameters, such as the line averaged density and the plasma stored energy [Fig. 1(a)]. This oscillation is typically reproducible in a particular line averaged density range, $\bar{n}_e \sim 5$–9×10^{19} m^{-3}. The oscillation ceases at $t \sim 4.1$ s when the density falls below the lower boundary.

Details of the divertor oscillation are shown in Fig. 2. Since oscillations in the neutral pressure and the electron temperature and density in the divertor region (not shown here) are all in phase, the recycling driven bifurcation model [6–8] may not explain the observation. This oscillation is considered to originate in the upstream plasma. Moreover, the oscillation observed here involves a clear magnetic activity, unlike the recycling driven divertor oscillation [23]. Time evolution of the plasma current is shown in Fig. 2(c). On a slowly varying trend mainly due to the beam driven current, a quick fluctuation highly correlated with the oscillation is clearly observed. Here the negative sign of the plasma current corresponds to the co-toroidal magnetic field direction. Note that the beam driven current has a radially broad profile, and does not affect the X-point current modulation being discussed below.

The relation between a proxy of the relative magnetic island width $\sqrt{\Phi/\Phi_{\rm ext}}$ and the X-point radiation intensity $P^X_{\rm rad}$ is shown in Fig. 2(d). When the magnetic island expands and reaches a critical value, the detachment transition occurs and the X-point radiation intensity abruptly increases (arrow A). In the divertor detachment phase, the magnetic island begins to shrink due to the detachment counteraction, which leads to the X-point radiation reduction (arrow B). Eventually, the divertor detachment is terminated, and the peripheral electron temperature may recover. Then, the magnetic island width again begins to increase (arrow C), which finally closes the loop of the divertor oscillation.

Figure 2(e) shows the relation between the island width and the oscillating part of the plasma current. A positive surge in the plasma current occurs when the magnetic island approaches its minimum in the attached phase (arrow B''), followed by a phase where the plasma current decreases and the magnetic island grows (arrow C). The trajectory mostly stagnates during the X-point radiation rise (arrow A). Then, the magnetic island in turn shrinks, during which the plasma current is more or less maintained (arrow B').

In order to examine the background physics of the self-sustained divertor oscillation, plasma profiles in the fully detached ($t = 3.70$–3.77 s) and attached ($t = 4.13$–4.20 s) phases are compared. Plasma profiles are measured by the Thomson scattering diagnostic, having sampling volumes at the midplane of a horizontally elongated plasma cross section, as shown in Fig. 3(a). Since the laser repetition rate for the Thomson scattering diagnostic is lower than the divertor oscillation frequency, plasma profile evolution during the divertor oscillation cannot be resolved. By applying the $m/n = 1/1$ RMP field, the O-point is formed at the bottom side in Fig. 3(a), and island flux surface contours extend beyond the midplane (where profile measurements in Fig. 3 are taken). In addition, the stochastic region at the periphery is significantly expanded, shortening the local connection length. Note that the distinct island separatrix is not formed in this configuration.

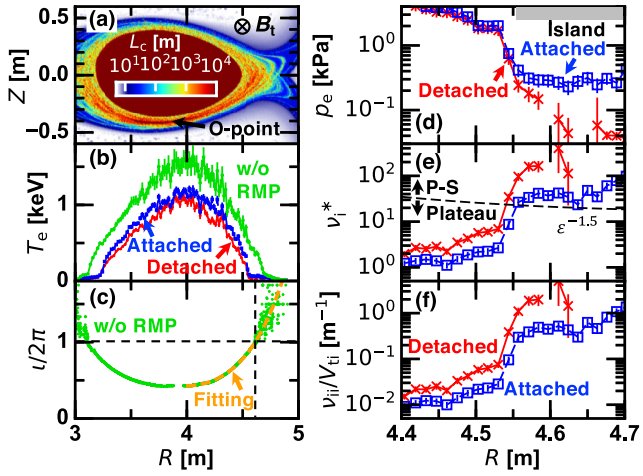


FIG. 3. (a) Connection length distribution for the poloidal cross section at which sample volumes for the Thomson scattering system are aligned at the $Z = 0$ m level, and radial profiles of (b) electron temperature, (c) vacuum rotational transform without RMP application and its fourth order even polynomial fit with respect to $R_{\rm ax}$, (d) electron pressure, (e) ion collisionality, and (f) inverse mean free path for attached and detached plasmas. Island flattening region is highlighted in (d). Dashed curve in (e) corresponds to $\epsilon^{-1.5}$, where ϵ is the inverse aspect ratio.

The electron temperature profile is flattened at the $\iota/2\pi = 1$ rational surface in the peripheral stochastic region, leading to a shrinkage of the plasma volume compared to a reference discharge where the RMP is not applied. In the detached phase, the electron temperature drops over the radius with respect to the attached phase. Particularly, the decrement is significant in the magnetic island region, approximately by a factor of 3. The electron pressure also falls down close to the diagnostic sensitivity limitation in the profile flattening region. As a result, the ion collisionality ν_i^* and the inverse mean free path ν_{ii}/V_{ti}, where ν_{ii} is the ion-ion collision frequency and V_{ti} is the ion thermal velocity, show overall increments. The electron pressure is also flattened both in detached and attached phases at the $\iota/2\pi = 1$ rational surface.

As a working hypothesis for the magnetic island width modulation, synchronized with the divertor oscillation, bootstrap current dynamics is examined. In high collisionality LHD plasmas, the bootstrap current is directed in such a way that the rotational transform is reduced [24]. In this situation, the bootstrap current is predicted to expand the magnetic island [25] analogous to the normal shear tokamak discharge case, as illustrated in Fig. 4(a). When a magnetic island is initiated either by the RMP or other mechanisms, the bootstrap current at the O-point disappears because of the electron pressure flattening and/or the increment in the collision frequency. The remnant bootstrap current at the X-point region having the $m/n = 1/1$ helical structure creates a radial magnetic field that is directed to enhance the original magnetic island. This mechanism is

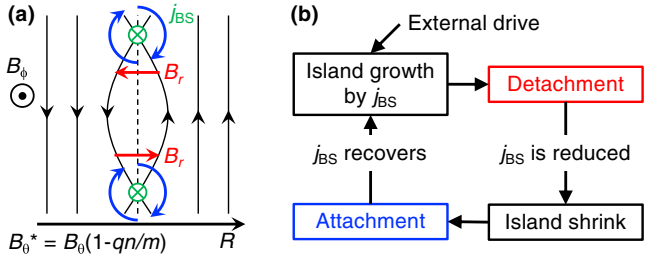


FIG. 4. (a) Schematic of remnant bootstrap current expanding magnetic island and (b) possible mechanism of self-sustained divertor oscillation.

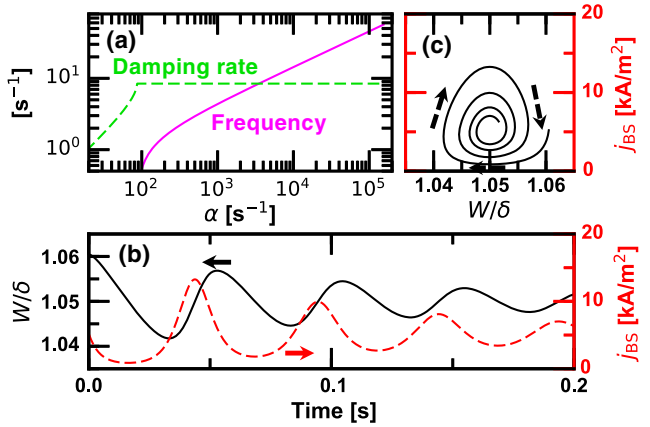


FIG. 5. (a) Frequency and damping rate of self-sustained divertor oscillation as a function of bootstrap current growth rate α, (b) time evolutions of normalized island width (W/δ) and bootstrap current density (j_{BS}) obtained numerically, and (c) Lissajous diagram of j_{BS} versus W/δ.

well formulated as the modified Rutherford equation [26] [shown Eq. (1) below], and successfully applied in the neoclassical tearing mode study [27–29]. In the present case, the plasma detachment needs to be additionally accounted for when the island width becomes large enough. The remnant bootstrap current is considered to be reduced after the detachment transition because the electron temperature at the X-point region drops, enhancing the radiation loss, as anticipated in [22]. The magnetic island in turn shrinks, leading to the attachment back transition. Then, the electron temperature at the X-point region and therefore the remnant bootstrap current recover, which again contribute to the magnetic island expansion. This closed loop is depicted in Fig. 4(b).

This hypothesis is examined by coupling the modified Rutherford equation to a heuristic model for the bootstrap current evolution in a predator-prey system as

$$\frac{\partial W}{\partial t} = V_M \frac{\delta^2}{W^2} - V_M + C\frac{j_{BS}}{W}, \tag{1}$$

$$\frac{\partial j_{BS}}{\partial t} = \alpha j_{BS} - \beta W j_{BS}, \tag{2}$$

where W is the magnetic island width, δ is the vacuum RMP island width, j_{BS} is the bootstrap current density, $V_M = |\Delta'| r_s^2 \tau_R^{-1}$ is the characteristic magnetic diffusion speed, and $C = 2r_s^2 \mu_0 |L_q| \tau_R^{-1} \langle B_p \rangle^{-1}$ is the coupling coefficient. Parameters in the coefficients are the minor radius of the rational surface $r_s = 0.52$ m, the resistive magnetic diffusion time $\tau_R = \mu_0 r_s^2/\eta_{NC}$ where η_{NC} is the neoclassical resistivity, the scale length of the safety factor $L_q = q(dq/dr)^{-1}$, and the flux surface averaged poloidal magnetic field $\langle B_p \rangle$. The tearing stability parameter $|\Delta'| \sim 2.4$ m^{-1} is obtained by integrating the MHD equation [27] with the measured boundary condition in a reference discharge where the RMP is not applied. Here the ion temperature is assumed to be equal to the electron temperature because of a high collisionality condition. Two unknowns are present: the linear growth rate of the bootstrap current α and the nonlinear saturation coefficient β.

The linear response of the system is examined by the perturbative expansion with $W = W_0 + W_1$ and $j = j_0 + j_1$, where the terms with subscripts 0 and 1 indicate zeroth order mean quantities and first order oscillatory quantities, respectively. The subscript "BS" is dropped from j_{BS} for simplicity. From the observation, $W_1/W_0 \sim O(0.1)$, therefore the perturbation quantities can be used as expansion parameters. One of the zeroth order fixed points is given as

$$(W_0, j_0) = (\alpha/\beta, W_0 V_M C^{-1}[1 - \delta^2 W_0^{-2}]). \tag{3}$$

As W_0 is observable in experiment, $\beta = \alpha/W_0$ and only one unknown α now remains. The corresponding first order equation gives the system eigenvalues,

$$\lambda = \frac{V_M}{2W_0}(1+\delta^2 W_0^{-2})\left[-1 \pm \sqrt{1 - \frac{4\alpha W_0}{V_M}\frac{1-\delta^2 W_0^{-2}}{1+\delta^2 W_0^{-2}}}\right], \tag{4}$$

which is a function of the bootstrap current growth rate α. The real part and the imaginary part of the eigenvalue correspond to the growth rate and the frequency of the system, respectively, and are shown in Fig. 5(a). The oscillation solution appears in $\alpha > 10^2$ s^{-1}, and the oscillation frequency becomes larger than the damping rate in $\alpha > 3 \times 10^3$ s^{-1}. A continuous oscillation is expected to appear if the bootstrap current growth rate is large enough, particularly in a high density edge plasma with high resistivity.

A system response with a finite oscillation amplitude is studied by numerically solving Eqs. (1) and (2) with a fourth-order Runge-Kutta scheme. For the parameter α, the inverse of the parallel diffusion time $(\nu_{ii}/V_{ti})^2 D_\parallel \sim 2 \times 10^4$ s^{-1} is used ($D_\parallel \equiv V_{ti}^2/\nu_{ii}$ being the ambipolar diffusion coefficient), which is a representative response timescale of the bootstrap current in the collisional regime [30]. Note

that the variation of the electron temperature profile is much faster because of a high parallel electron diffusivity. The initial value for W that determines the amplitude of the response is given to match the experimental observation, while the fixed point value of j_0 is given as the initial value for j. The result of the simulation is shown in Figs. 5(b) and 5(c). The model results are in good qualitative agreement with the experimental observation depicted in Fig. 2, except for the damping property in the oscillation amplitude. The obtained system frequency of ~20 Hz is only a factor of 2 smaller than the experimental value. A modulation amplitude of $\sim 10\ \mathrm{kAm}^{-2}$ in j also agrees with the theoretically expected value of $\mathcal{D}dp/dr \sim 10\ \mathrm{kAm}^{-2}$ in the neoclassical transport study, where $\mathcal{D}$ is the dimensionless bootstrap current coefficient [24]. Moreover, considering the cross section where the modulated bootstrap current flows [22], the expected amplitude in the total plasma current is given as ~0.3 kA, which also coincides with the experimental case [Fig. 2(e)].

At present, the simplest model Eq. (2) was chosen for intuitively describing the bootstrap current dynamics. Although it was sufficient for a qualitative discussion where the oscillation amplitude was small, a more realistic model, including nonlinear detachment-attachment transition, might be necessary for a better reproduction of the experimental trend. Reproducing the constant amplitude oscillation, possibly having a limit-cycle trajectory, is also an important issue. Moreover, parameter dependence of the oscillation properties, in particular the frequency and the amplitude, needs to be experimentally examined in the future.

In conclusion, a self-sustained divertor oscillation was discovered in the resonant magnetic perturbation assisted detachment discharge in LHD. The divertor oscillation was found to be a self-regulation of the magnetic island width, induced by a drastic change of the X-point plasma parameters across the detachment-attachment transitions. A predator-prey model between the magnetic island width and the bootstrap current was introduced to describe the divertor oscillation, which successfully reproduced the experimental observations. According to the proposed model, a stable detachment is foreseen in a reactor relevant collisionless plasma.

The LHD data can be accessed from the LHD data repository [31].

The authors thank the LHD experiment group for their assistance, and K. Ida, M. Osakabe, and S. Masuzaki for strong support. This work is partly supported by the JSPS Grant-in-Aid for Scientific Research (No. 17K14898 and No. 21K13902, and No. 19H01878) and the NIFS grants (ULHH033 and ULPP026).

[1] L. Wang *et al.*, Nat. Commun. **12**, 1365 (2021).
[2] A. W. Leonard, Plasma Phys. Controlled Fusion **60**, 044001 (2018).
[3] M. Kobayashi *et al.*, Nucl. Fusion **53**, 093032 (2013).
[4] D. Zhang *et al.*, Phys. Rev. Lett. **123**, 025002 (2019).
[5] A. E. Jaervinen *et al.*, Phys. Rev. Lett. **121**, 075001 (2018).
[6] A. Loarte, R. D. Monk, A. S. Kukushkin, E. Righi, D. J. Campbell, G. D. Conway, and C. F. Maggi, Phys. Rev. Lett. **83**, 3657 (1999).
[7] P. Heinrich *et al.*, Nucl. Fusion **60**, 076013 (2020).
[8] S. I. Krasheninnikov, A. S. Kukushkin, and A. A. Pshenov, Phys. Plasmas **23**, 055602 (2016).
[9] R. D. Smirnov, A. S. Kukushkin, S. I. Krasheninnikov, A. Yu. Pigarov, and T. D. Rognlien, Phys. Plasmas **23**, 012503 (2016).
[10] T. W. Petrie, T. E. Evans *et al.*, Nucl. Fusion **51**, 073003 (2011).
[11] H. Frerichs, O. Schmitz, X. Bonnin, A. Loarte, Y. Feng, L. Li, Y. Q. Liu, and D. Reiter, Phys. Rev. Lett. **125**, 155001 (2020).
[12] M. Jia, A. Loarte *et al.*, Nucl. Fusion **61**, 106023 (2021).
[13] Y. Nagayama *et al.*, Nucl. Fusion **45**, 888 (2005).
[14] Y. Narushima, K. Y. Watanabe, S. Sakakibara, K. Narihara, I. Yamada, Y. Suzuki, S. Ohdachi, N. Ohyabu, H. Yamada, and Y. Nakamura, Nucl. Fusion **48**, 075010 (2008).
[15] B. L. Peckarsky *et al.*, Ecology **89**, 2416 (2008).
[16] E. Aydiner, Sci. Rep. **8**, 721 (2018).
[17] A. E. Ross and D. R. McKenzie, Sci. Rep. **6**, 24040 (2016).
[18] E. J. Kim and P. H. Diamond, Phys. Rev. Lett. **90**, 185006 (2003).
[19] M. Kobayashi *et al.*, Nucl. Fusion **59**, 096009 (2019).
[20] H. P. Furth, P. H. Rutherford, and H. Selberg, Phys. Fluids **16**, 1054 (1973).
[21] M. Kobayashi *et al.*, Phys. Plasmas **17**, 056111 (2010).
[22] M. Kobayashi and M. Z. Tokar, Contrib. Plasma Phys. **60**, e201900138 (2020).
[23] M. Cavedon *et al.*, Nucl. Fusion **60**, 066026 (2020).
[24] M. Y. Isaev, K. Y. Watanabe, M. Yokoyama, N. Ohyabu, C. D. Beidler, H. Maassberg, W. A. Cooper, T.-M. Tran, and M. I. Mikhailov, Plasma Fusion Res. **3**, 036 (2008).
[25] K. Itoh, S.-I. Itoh, and M. Yagi, Phys. Plasmas **12**, 072512 (2005).
[26] R. Carrera, R. D. Hazeltine, and M. Kotschenreuther, Phys. Fluids **29**, 899 (1986).
[27] Z. Chang, J. D. Callen, E. D. Fredrickson, R. V. Budny, C. C. Hegna, K. M. McGuire, M. C. Zarnstorff, and TFTR group, Phys. Rev. Lett. **74**, 4663 (1995).
[28] D. A. Gates, B Lloyd, A. W. Morris, G. McArdle, M. R. O'Brien, M. Valovic, C. D. Warrick, and H. R. Wilson, Nucl. Fusion **37**, 1593 (1997).
[29] A. Isayama *et al.*, Nucl. Fusion **47**, 773 (2007).
[30] Z. Lin, W. M. Tang, and W. W. Lee, Phys. Plasmas **2**, 2975 (1995).
[31] https://www-lhd.nifs.ac.jp/pub/Repository_en.html.